An Initial Assessment of the Performance Achieved by the Seasat-1 Radar Altimeter

WILLIAM F. TOWNSEND

Abstract—**This paper describes the results of an initial on-orbit engineering assessment of the performance achieved by the radar altimeter system flown on Seasat-1. Additionally, the general design characteristics of this system are discussed and illustrations of altimeter data products are provided. The instrument consists of a 13.5-GHz monostatic radar system that tracks in range only using a 1-m parabolic antenna pointed at the satellite nadir. Two of its unique features are a linear FM transmitter with 320-MHz bandwidth, which yields a 3.125-ns time-delay resolution, and microprocessor-implemented closed-loop range tracking, automatic gain control (AGC), and real-time estimation of significant wave height (SWH). Results presented herein show that the altimeter generally performed in accordance with its original performance requirements of measuring altitude to a precision of less than 10-cm rms, SWH to an accuracy of ±0.5 m or 10 percent whichever is greater, and ocean backscatter coefficient to an accuracy of ± 1 dB, all over an SWH range of 1 to 20 m.**

I. INTRODUCTION

THE SEASAT-1 spacecraft was placed into earth orbit on June 27, 1978. A radar altimeter, part of this ocean dedicated satellite instrumentation system represented the first attempt to achieve 10-cm altitude precision from orbit. Functionally, the altimeter measures the spacecraft height above mean sea level (MSL), and the significant wave height (SWH) and backscatter coefficient (σ°) of the ocean surface beneath the spacecraft. It contributes to the overall Seasat objectives of demonstrating global monitoring of wave height; detecting currents, tides, and storm surges; and mapping the global ocean geoid. The instrument consists of a 13.5-GHz monostatic radar system that tracks in range only using a 1-m parabolic antenna pointed at the satellite nadir. One of its unique features is the microprocessor implementation of the closed-loop range tracking, automatic gain control (AGC), and real-time estimation of SWH. Additionally, a linear FM transmitter with 320-MHz bandwidth yields a 3.125-ns time-delay resolution. This high resolution, coupled with a high transmitted pulse rate of 1020 Hz, permits the realization of the desired 10-cm altitude precision.

The altimeter was turned on for the first time on July 3, 1978, and declared operational on July 7, 1978. Subsequent to this, a detailed assessment/analysis of performance was conducted. Coupled with this activity, various surface truth data collecting activities were conducted in an attempt to evaluate/calibrate the real-time wave-height measurement. After this initial engineering assessment period, global altimeter data continued to be collected until October 10, 1978, when a massive short circuit in the spacecraft power system prematurely terminated the Seasat mission after only 99 days of sensor operations. Nonetheless, due to the on-board recording capability, some 1684 h of high quality altimeter data were collected. As a point of comparison, this represents about 90 percent of the data collected by the GEOS-3 Radar Altimeter during its 3 $\frac{1}{2}$ years of real-time operation.

This paper describes the altimeter and summarizes the results of the initial on-orbit engineering performance assessment. A more in-depth treatment of the engineering performance assessment can be found in [1], and to some extent, the information contained herein represents summaries and/or extractions taken from that document.

A. Background

Satellite altimetry is devoted to the active remote sensing of the ocean surface and thereby represents an important new source of measurements. These measurements are sufficient to provide all-weather independent observations of global topographic features, thus contributing to the accurate mapping of underwater features and the detection and measurement of ocean currents, tides, and storm surges, as well as the monitoring of wave height on a global basis.

The long-term objectives of satellite altimetry were stated in the 1969 Williamstown study on Solid Earth and Ocean Physics [2]. Basically, the development of a satellite altimeter system having a topographic precision of ± 10 cm or less was called for. It was felt that this level of precision would permit detection of global circulation patterns.

The Skylab S-193 Altimeter was the first in the series of satellite altimeters that were planned to progressively achieve this goal. This altimeter was designed primarily for obtaining the radar measurements necessary for designing improved altimeters. The GEOS-3 Altimeter, second in the series of satellite altimeters, was launched on April 9, 1975, and was the first globally applied altimeter system. The Advanced Aplications Flight Experiments (AAFE) Altimeter, an aircraft system which first collected data in October 1975, was a developmental effort directed at bridging the technology gap between the capabilities of the GEOS-3 Altimeter and the rather stringent requirements imposed on the Seasat-1 Altimeter as well as providing surface truth in support of Seasat-1 Altimeter calibration activities. The Seasat-1 Altimeter, third in the series of satellite altimeters, was part of an ocean dedicated satellite instrumentation system and represented the first attempt to achieve 10-cm precision from orbit. It is conceptually identical to the AAFE Altimeter.

Manuscript received October 31, 1979; revised December 15, 1979.
The author is with NASA Wallops Flight Center, Wallops Island, VA 23337.

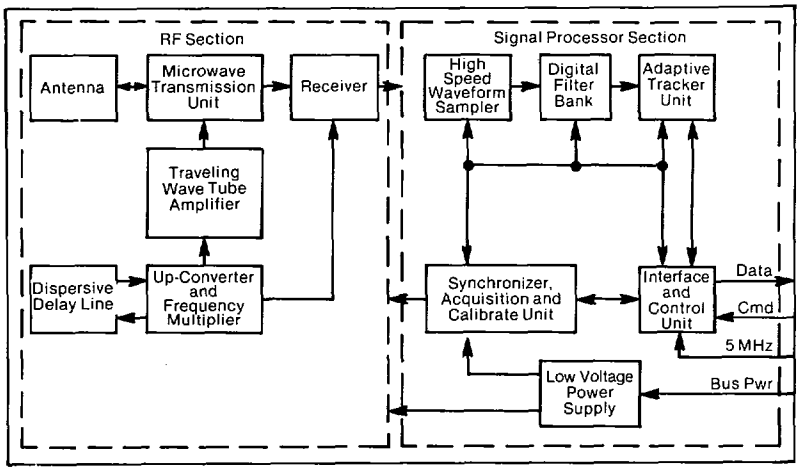

Fig. 1. Seasat-1 Radar Altimeter major functional elements [6].

II. ALTIMETER DESCRIPTION

To provide the reader with a good general understanding of the altimeter design, particularly as it affects his interpretation of the results of the on-orbit engineering performance assessment presented herein, pertinent design details have been summarized and/or extracted from [3]-[6] and are presented in the following sections.

A. Altimeter Performance Requirements

Based on geophysical measurement requirements specified by the general oceanographic and geodetic user community [7], the following key altimeter performance requirements were derived and used to arrive at a suitable design for the altimeter.

1) At an output rate of one height measurement data point per second, the noise level of these data points shall be such that 68 percent of the data points lie within ± 10 cm of the fitted mean.
2) At an output rate of one measurement per second, the altimeter shall provide a measurement of the SWH of the ocean surface beneath the spacecraft. The absolute accuracy of this measurement shall be at least ± 10 percent of SWH or 0.5 m, whichever is greater.
3) The altimeter shall provide information concerning the measurement of the backscatter coefficient (σ°) of the ocean surface beneath the spacecraft, i.e., normal incidence. When subjected to appropriate ground processing, this information shall result in the measurement of σ° to an absolute accuracy of at least ± 1.0 dB.

It was a further requirement that 1), 2), and 3) be satisfied over an SWH range of 1 to 20 m.

B. Resulting Altimeter Design

The Johns Hopkins University/Applied Physics Laboratory (APL), under the direction of NASA Wallops Flight Center, designed, fabricated, and tested the radar altimeter system flown on the Seasat-1 spacecraft. The altimeter was physically divided into two packages, an RF section with attached antenna and a signal processor section. The envelope dimensions of the RF section, including the antenna, are 1.048 m in diameter by 0.781 m high. The signal processor section is 50.8 cm long by 34.2 cm wide by 25.3 cm high. The two packages are electrically interconnected through a 2.13-m set of cables. The total weight of the altimeter is 93.8 kg. The total dc power required at the nominal spacecraft bus voltage of 28 Vdc is 165 W. A block diagram depicting the major functional elements of the system is shown in Fig. 1. Each of these elements is described in more detail below.

The dispersive delay line (DDL) generates the basic linear FM (chirp) pulse. The heart of the DDL is a surface acoustic wave (SAW) device fabricated on a lithium tantalate substrate. At a pulse repetition frequency (PRF) of 1020 Hz, the associated electronic applies a 12.5-ns impulse at a 250-MHz-center frequency to the SAW filter, which then generates an expanded chirp pulse having the characteristic of linearly decreasing frequency within a bandwidth of 80 MHz and a time interval of 3.2 μs. Subsequent X4 multiplication will increase the pulse bandwidth to 320 MHz.

Utilizing the spacecraft 5-MHz reference signal, the up-converter/frequency multiplier (UCFM) generates all RF signals required to convert the DDL output pulse to the required transmit drive and local oscillator pulses. During the transmit mode, the chirp pulse from the DDL at 250 MHz is converted to 3375 MHz, amplified to the 1-W level, and multiplied X4 to 13.5 GHz, thus achieving the desired 320-MHz chirp pulse bandwidth. In the receive mode, the DDL chirp pulse is converted to 3250 MHz and amplified to about 100 mW before X4 multiplication to 13.0 GHz. Additionally, under control of an external signal, the UCFM switches in a CW signal in place of the DDL chirp pulse as required for the altimeter acquisition mode.

The traveling wave tube amplifier (TWTA) consists of a high voltage power supply/modulator and an external TWT. The TWT is a Hughes 852H which was also used on the Skylab S-193 and GEOS-3 Altimeter missions. The TWTA amplifies the UCFM transmit drive pulse to the 2-kW level. A pulsewidth of 3.2 μs and a PRF of 1020 Hz yields a duty cycle of 0.33 percent which corresponds to 6.5 W of average radiated RF power.

The microwave transmission unit (MTU) provides the waveguide interconnection between the antenna, transmitter,

and receiver. A key element is a five-port circulator that provides for transmit/receive mode switching as well as calibration mode switching. In the transmit mode, the 2-kW TWTA output pulse is switched directly to the antenna. In the receive mode, the incoming return signal from the ocean surface is switched directly from the antenna to the receiver. In the calibrate mode, the transmitter is switched to an internal load and a controlled sample is coupled to the receiver via a digital step attenuator. To minimize RF losses, the first mixer function of the receiver is also accomplished in the MTU. Full deramping is achieved by mixing the 13.5-GHz incoming chirp signal with a 13.0-GHz local oscillator chirp signal resulting in a 500-MHz intermediate frequency (IF) for output to the receiver.

The antenna is a 1-m diameter horn-fed parabolic dish yielding a nadir directed gain of 40.8 dB and a one-way 3-dB beamwidth of 1.59°. The beamwidth limited footprint associated with this antenna is circular in shape, centered on the spacecraft nadir, and has a diameter of 22.2 km from the nominal spacecraft altitude of 800 km. The effective pulse-width limited footprint of 1.6-km diameter for a smooth surface is contained well within the beamwidth limited footprint.

Signals received at the 500-MHz IF from the MTU are mixed in the receiver with a 500-MHz CW second local oscillator to form in-phase and quadrature (I and Q) video signals for use in the digital filtering scheme. The 500-MHz IF signal is also detected prior to the second mixer for use when CW (unchirped) pulses are transmitted in the acquisition mode. Receiver gain control (AGC) is provided via a digital step attenuator over a 0–63-dB range in 1-dB steps under microprocessor control.

The I and Q video signals from the receiver are A/D converted and stored for further processing in the high speed waveform sampler (HSWS). Conversion takes place at 20 MHz and precisely 64 samples of each video signal are taken over a 3.2-μs interval using a five-bit A/D converter. Readout of the stored samples to the digital filter bank (DFB) takes place at a 10-MHz rate.

The DFB operates on the samples read out of the HSWS in the interval between received pulses to form a bank of 60 contiguous filters by implementing a phase rotation algorithm in conjunction with sine and cosine READ-ONLY memories. Each filter has a bandwidth of 312.5 kHz which corresponds to the basic 3.125-ns resolution of the system. Square law detection is done in a READ-ONLY memory which outputs the square of the input. As each filter output is formed, it is read out serially to the adaptive tracker unit (ATU).

The ATU is a microcomputer built around an Intel 8080 microprocessor. The READ-ONLY program memory consists of 4096 eight-bit bytes and the READ-WRITE storage memory consists of 2048 eight-bit bytes. Dual buffers alternately accumulate waveform sample data from the DFB for 50 pulse returns and hold the data for processing by the microprocessor. Height tracking, AGC, and wave-height estimation is then done at a 20/s rate based on the smoothed waveform samples. Telemetry (TM) data formatting, interpretation of commands, and control of altimeter mode sequencing between acquisition, track, and calibrate states are also accomplished within the ATU.

The synchronizer/acquisition/calibrate unit (SACU) combines several related functions into a single unit. Basic timing waveforms are generated by counting down an 80-MHz oscillator locked to the spacecraft 5-MHz reference. Based on inputs from the ATU, control signals are passed to the RF section which set up the desired signal conditions and mode switching as a function of current acquisition, track, or calibrate states. A precision digital delay generator counts down coarse height and initiates receive processing including the retriggering of the DDL chirped pulse. Finally, the SACU maintains a threshold detector and range counter which is operative in the acquisition mode and reports the height of CW mode detections to the ATU.

The interface and control unit (ICU) provides the electrical interface with the spacecraft for all telemetry and data command signals. Latching relays for pulse commands are located in the low voltage power supply (LVPS). Data commands are latched by an instrument unique strobe pulse and transmitted via a serial interface to the ATU. TM formatting for all science and engineering data is done in the ATU and then output to the ICU for spacecraft interfacing.

The LVPS supplies seven regulated voltages to RF section and signal processor section circuits. Regulation over input bus variations from 24 to 32 V is 1 percent. The overall efficiency of the LVPS is 80 percent.

C. Microprocessor Implementation of Key Measurement Functions

As noted previously, height tracking, AGC, and wave-height estimation are all accomplished under ATU control. Further discussion of the algorithms used follows.

1) For the purpose of maintaining a constant output level and to insure operation within the linear region of all receiver stages, an AGC loop is implemented in the altimeter. A digital attenuator in the receiver provides for a gain variation of 0–63 dB in 1-dB steps. In the absence of signal, the overall gain is adjusted by fixed pads so that an AGC attenuator setting of 10 dB is observed. This leaves a range of 53 dB above noise for signal variation. For σ° between 10 and 15 dB, the corresponding AGC setting would be between 28 and 33 dB. The remaining AGC range allows for increases typical of near-specular returns from ice, lakes, very calm water, or other smooth surfaces.

Implementation of the AGC is such that the average of all 60 waveform samples is driven to a constant. The prime motivation for basing AGC control on the average of all waveform samples was the desire to hold the rms level of the I and Q video signals to a constant regardless of the shape of the return signal. This avoids saturation when near-specular or overland returns alter the shape of the return signal. It should be noted that the AGC gate formed in this way has an effective footprint diameter of 9.5 km [6]; signals from islands or nearby land falling within this circle will have an effect on AGC and height error (described below) that is derived from the AGC gate.

AGC processing is shown in Fig. 2. Digital filter bank

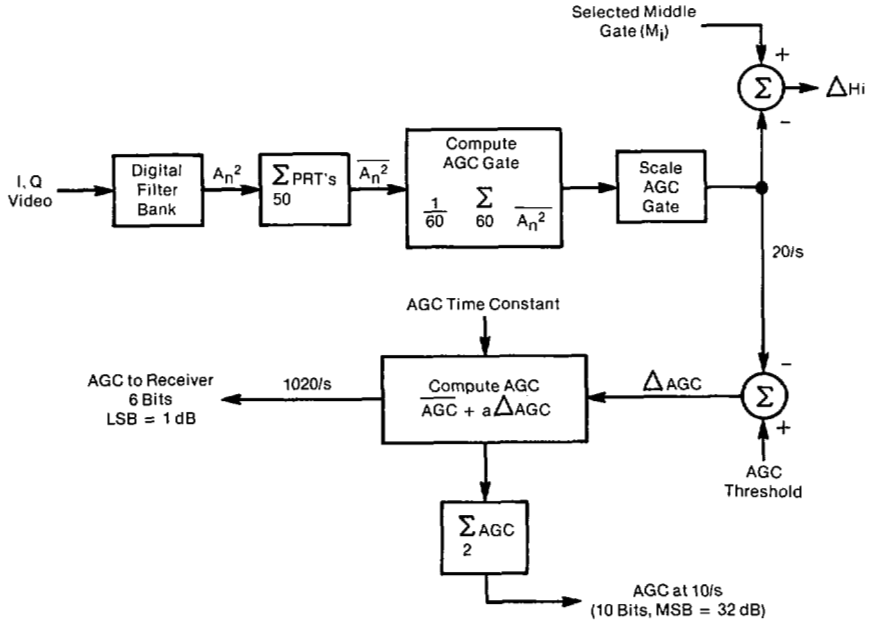

Fig. 2. AGC processing flow [6].

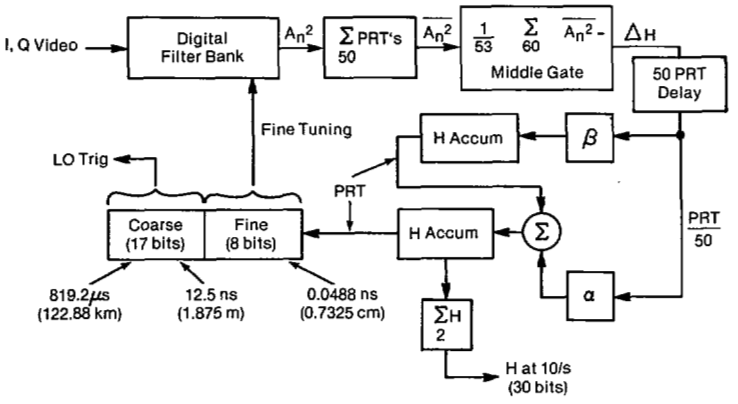

Fig. 3. Height processing flow [6].

(waveform sample) outputs are averaged over 50 successive returns prior to AGC gate formation. The AGC gate is scaled to account for the exponential antenna pattern falloff so that its amplitude corresponds to the half-power point on the leading edge of the signal.

The AGC gate is compared to a fixed constant and the difference (error signal) is scaled and added to the previous value to form an updated smoothed AGC word. The loop is closed via the digital attenuator in the receiver. While the LSB for gain control is 1 dB, finer bits are carried in the AGC word for smoothing and the result is an interpolated value with an LSB of 1/16 dB. The TM output at 10/s averages two consecutive updated AGC words.

2) The height processing function is accomplished by operating on the waveform sample outputs from the digital filter bank to implement a second-order α-β tracking loop. Waveform sample averaging over 50 consecutive returns precedes the development of a height error signal; thus the loop is updated at a 20/s rate. This rate was chosen to minimize the processing time required in the adaptive tracker and still allow tracking loop time constants as low as a few tenths of a second.

Referring to Fig. 3, operating on the averaged waveform samples, the height tracker forms a range error by subtracting the amplitude of a middle gate (chosen as a result of the wave-height estimation described subsequently) from the AGC gate formed by averaging all 60 waveform samples. As previously stated, scaling on the AGC gate accounts for the antenna pattern decay to give an amplitude to the half-power point on the return signal leading edge. For perfect height alignment the middle gate amplitude will also equal the half-power signal amplitude; misalignment will result in a positive or negative signal which can be related to the magnitude of the misalignment in time.

Based on waveform sample data averaged for 50 radar pulse time intervals (PRT), the adaptive tracker processes the samples to form gates, estimates wave height, computes a height error, and updates the previous height and height

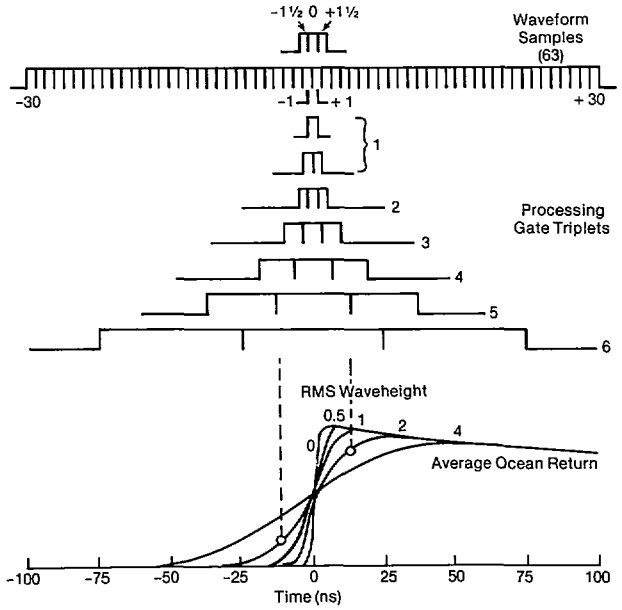

Fig. 4. Formation of processing gates from waveform samples [6].

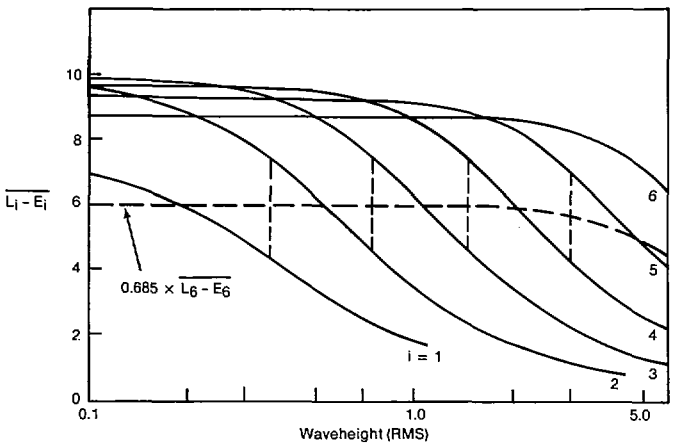

Fig. 5. Wave-height estimation [6].

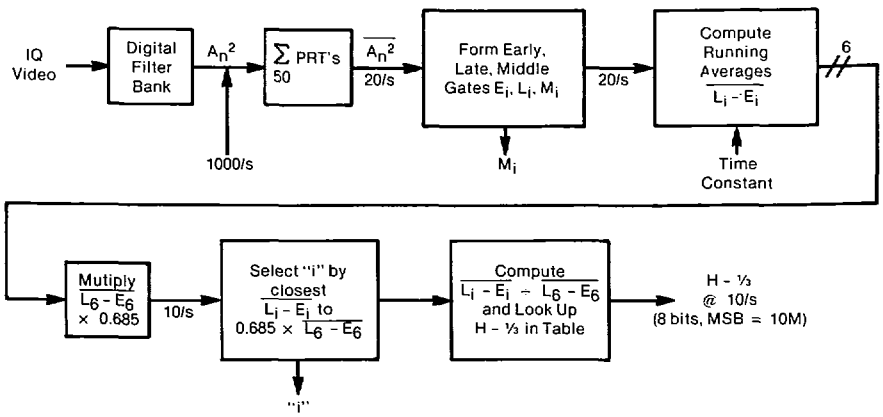

Fig. 6. Wave-height processing flow [6].

rate estimates in the following 50-PRT interval. Although loop updating takes place at a 20/s rate, the height word is made to step smoothly in between updates by applying rate corrections each radar pulse. At 50-m/s height rate, the height changes 2.5 m in 50 ms, thus the need for continuous updating.

A 25-bit height word is output from the ATU to the SACU each radar pulse. The eight fine bits are passed to the DFB where they are used to locate the precise center frequency of the filter bank. The 17 coarse bits are used to count down an 80-MHz clock to derive a trigger for regenerating the chirped local oscillator pulse. Tracking is ambiguous in that the overall delay for an 800-km height is 5333 μs. Signal return for a given transmit pulse will fall between the 5th (4900 μs) and 6th (5880 μs) succeeding pulse. The height word output to the TM system at the 10/s rate will be the result of averaging two successive updated height words.

3) Estimation of SWH begins with the formation of a set of processing gates as suggested in Fig. 4. By combining the outputs from contiguous 3.125-ns waveform samples, gate triplets of successively increasing width are formed. The early and late gates will enter into wave-height processing; the middle gate is used in height tracking once a gate triplet has been selected.

A signal formed by differencing the late and early gate amplitudes provides a measure of the slope of the ocean return signal leading edge. Adaptive selection of the operative gate pair matches the gate spacing (in X2 steps) to the signal slope to maximize the sensitivity to wave-height variation. This is further illustrated in Fig. 5. Plotting the six gate-pair difference signals versus wave-height results in the family of curves shown. The dashed curve formed by multiplying $(L_6 - E_6) \times 0.685$ provides a reference to which the remaining five gate-pair difference amplitudes are compared. At any given wave height, one pair will be closest in amplitude to the reference. The vertical dashed lines denote boundaries at which two adjacent pairs will be equally close to the reference. Within these boundaries the amplitude variation of the selected pair closest to the reference provides a vernier indication of wave height. A table of 16 entries spanning the operative region, plus some overlap, is provided for each of the five gate selections or a total of 80 entries.

The signal flow for wave-height processing is further illustrated in Fig. 6. Running averages are continuously main-

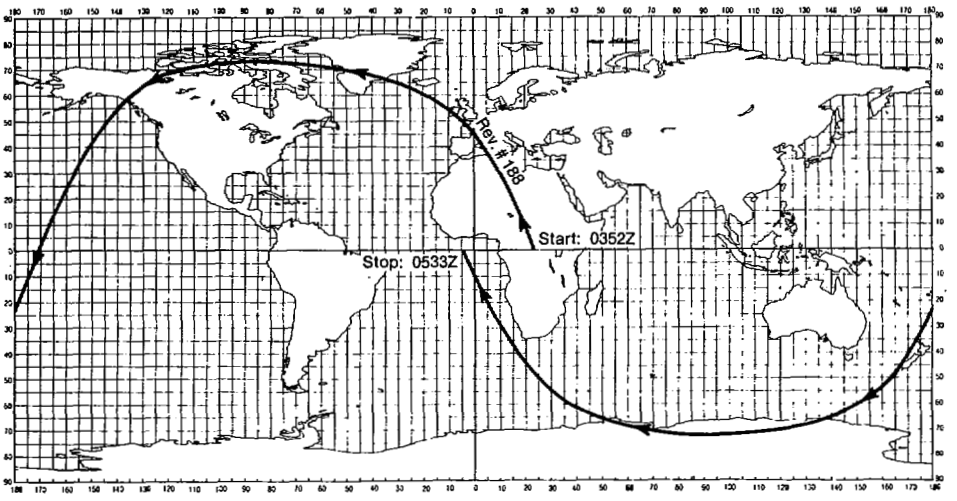

Fig. 7. Ground track for rev #188.

tained for all six gate-pair difference signals. The wave-height estimation process is based on the normalized ratio $\overline{L_i - E_i} \div \overline{L_6 - E_6}$ which avoids dependence on signal-to-noise ratio. The process results in very nearly constant percentage increments in SWH, which are never greater than 8 percent. Averaging SWH readouts at 10/s over longer periods will further reduce this quantization noise. Generation of the table lookup entries from the ocean return model is described in [8], and was in turn based on the derivations given in [9].

III. ALTIMETER ON-ORBIT PERFORMANCE

Our assessment/analysis of altimeter data to date has revealed that, with minor exceptions, the altimeter performed nominally throughout the life of Seasat. The altimeter is felt to generally have performed in accordance with the original specification and certainly in accordance with pre-launch expectations. This is despite the fact that the altimeter occasionally had to operate in the presence of random attitude disturbances, outside its designed temperature range of operation, and at spacecraft bus voltages below its designed minimum. The only known altimeter hardware anomaly was the "transmitter power dropout" problem which, while it certainly was a cause for concern, in no way impacted the quality of the altimeter data collected, since the transmitter dropouts were always over land and for short durations (<5 s).

The following sections present selected results from our overall engineering assessment activities. Generally, the data presented is representative of normal altimeter performance; additionally, as pertinent, specific features or capabilities of the altimeter and its data products are presented.

A. Typical Global Performance

Presented below is a full-rev global set of altimeter data taken during rev #188 on July 10, 1978. This rev was not chosen for any particular reason, but rather is felt to represent typical normal altimeter operations. Referring to the ground track shown in Fig. 7, rev #188 starts over the middle of Africa and progresses westward. Continuous altimeter data was collected during this period, selected parameters of which are plotted in Figs. 8 and 9.

If the orbital height derived from tracking data is subtracted from the altimeter measured height, the residual represents the height of the surface above the reference ellipsoid which is plotted at the top of Fig. 8 (scale of −200 to +3200 m). Note that the surface height associated with Antarctica and Greenland stands out. If the land data is then edited out and the scale is expanded to ±90 m, a plot of sea surface height is obtained as shown on the bottom graph. The undulations shown represent the global geoid with departures therefrom representing tides, storm surges, currents, baratropic effects, etc.

Continuing with the same data set shown at the top of Fig. 9 is a plot of the noise level of the height data over water. Note the 10-cm specification line shown. The noise level was computed by doing a first-order fit (to remove the rate) to a major frame of data (4.5 s), and then computing the standard deviation of the individual 10/s data points about the fit. This, then, represents a worst case approach to computing this parameter. If the data were smoothed over 1-s intervals (more in keeping with the specification), better results should be obtained and in fact, this is the case as will be shown in the next section. Still, by and large, the raw, unsmoothed data appears to have a noise level between 6 and 10 cm, with the higher values occurring at higher sea states as would be expected.

Shown next is the real-time SWH measurement on a scale of 0–12-m SWH. It has been edited so that the data shown is over water only. As might be expected global sea states are typically below 4-m SWH, with those excursions above representing storms. In particular note the storm centered at 0516 GMT between Antarctica and Africa and having a peak SWH of 11 m. Selected data obtained during this storm was utilized extensively during our performance assessment.

The bottom plot shows the backscatter coefficient (σ°) obtained over the full data set, i.e., land, water, and ice. Note particularly the double peaked high amplitude values of σ° seen over Antarctica. These indicate the presence of sea ice surrounding Antarctica, and data of this sort could be used to construct ice boundary maps much as was done with the GEOS-3 Altimeter [10].

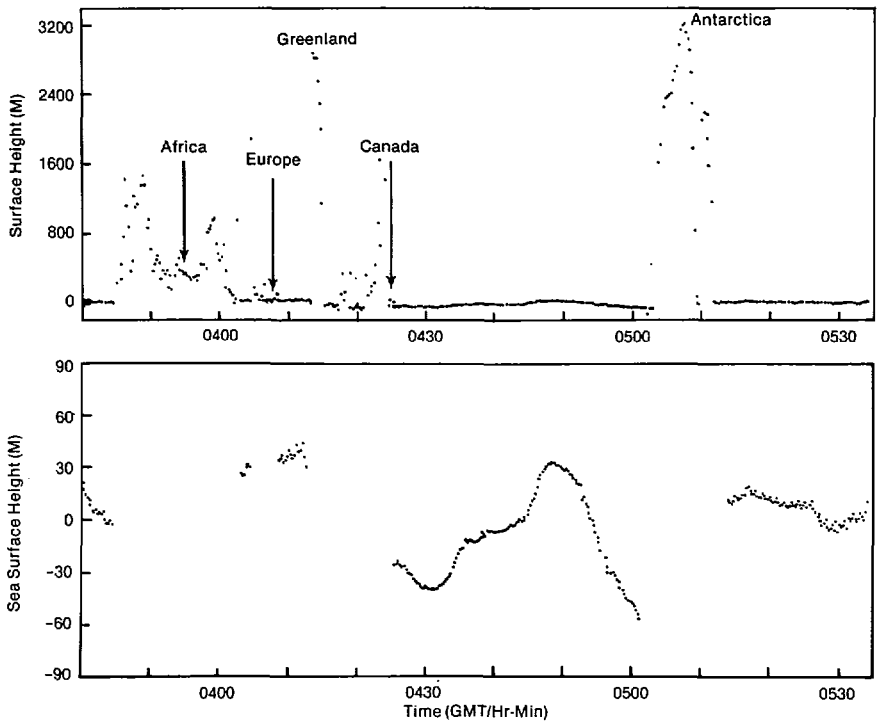

Fig. 8. Altimeter measurements during rev #188.

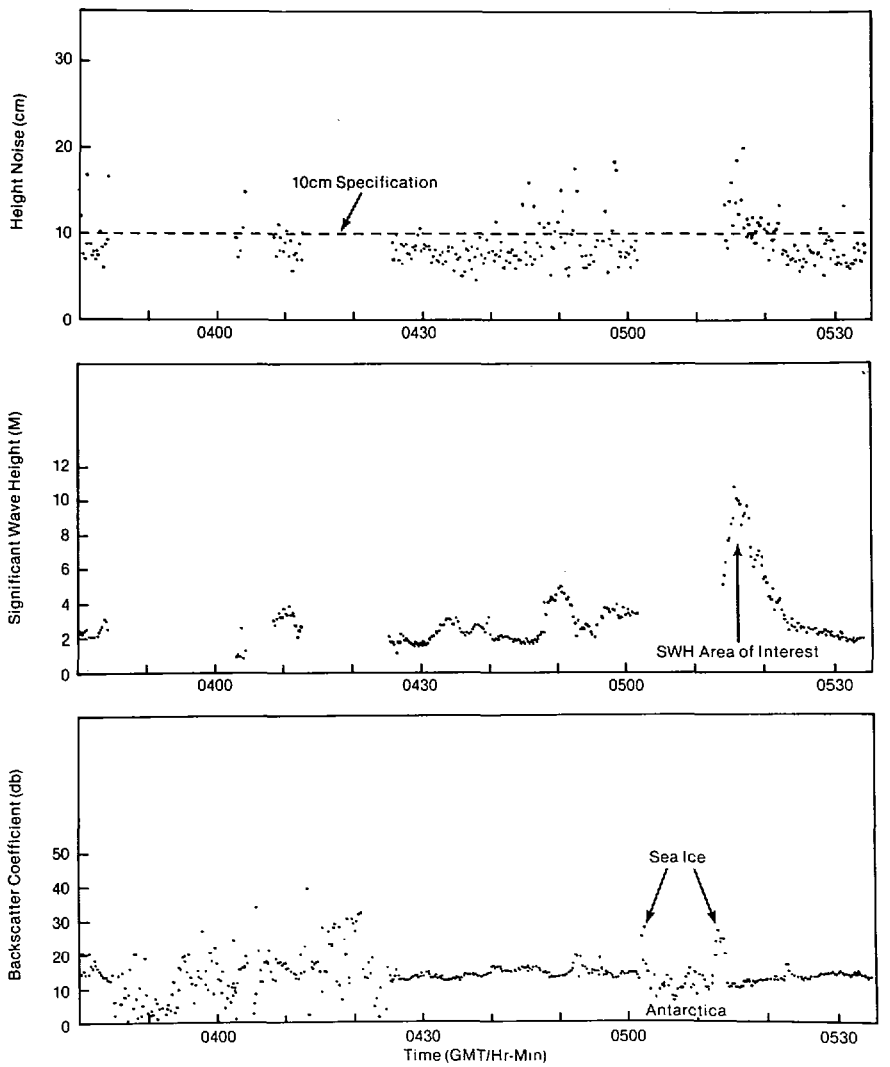

Fig. 9. Altimeter measurements during rev #188 (continued).

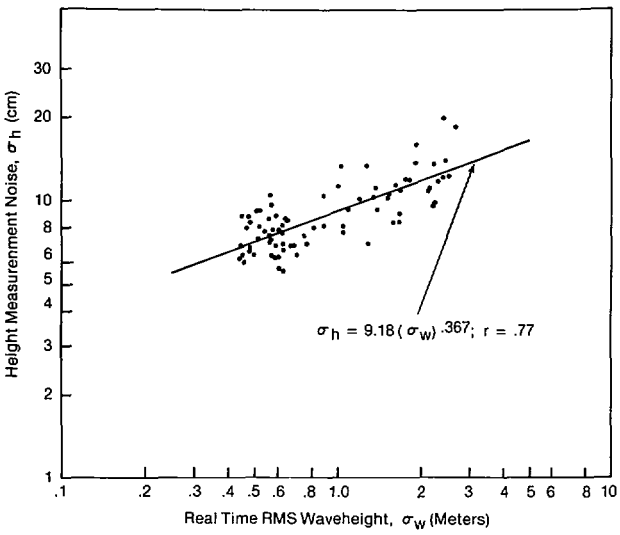

Fig. 10. Height measurement performance (no smoothing).

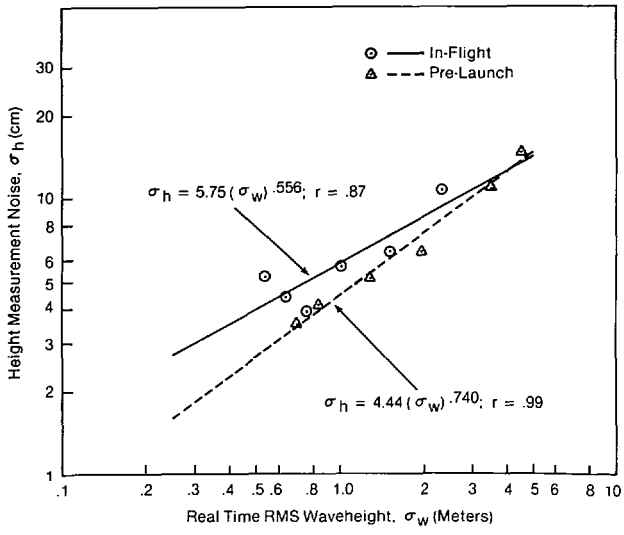

Fig. 11. Height measurement performance (one second smoothing).

B. Height Measurement Performance

Perhaps the most important performance specification placed on the altimeter design was the requirement to provide height measurements over a range of SWH of 1 to 20 m having a noise level of 10-cm rms or less based on 1-s averaging. This, then, sets the basic precision, or ability to detect changes in sea surface height due to currents, geoid, tides, etc., at the 10-cm level. How well the altimeter performed relative to this requirement has been the subject of extensive analysis. For the purposes of this paper, the storm shown in Fig. 9 centered at 0516 GMT on rev #188 on July 10, 1978, and occurring over the South Atlantic between Antarctica and Africa has been selected for demonstrating actual on-orbit performance since it covers a reasonably large range of SWH (2 → 11 m), the parameter to which height noise is most sensitive.

Fig. 10 is a plot of height noise versus rms wave height during the storm. Note that rms wave height is related to SWH by σ_w = SWH/4 [11]. A power curve has been fit to the data with good results. Note the tightness of the scatter. Also note that the altitude noise increases with SWH as expected. As can be seen it fails to meet the performance specification for SWH > 5 m. But, statistically, 70 percent of the global sea states are below 4 m, and therefore the performance achieved is considered quite adequate. This is especially true when one considers that the method of computing σ_h is the same as noted in the previous section and represents a worse case approach. In effect what is shown is the noise level of the raw 10/s data, i.e., without the benefit of any smoothing. If this same data set is smoothed (averaged) over a 1-s interval prior to computing the σ with respect to the fit, the result is as shown in Fig. 11. While an improvement of $\sqrt{10}$ might be expected, the maximum improvement realized is a factor of 2.2 for low SWH thus indicating that successive height measurements at the 10/s rate are somewhat correlated. As a point of comparison, the pre-launch test results using 1-s smoothing are also shown.

To demonstrate the utility of the height measurement as derived from Seasat-1 Altimeter data, some examples follow:

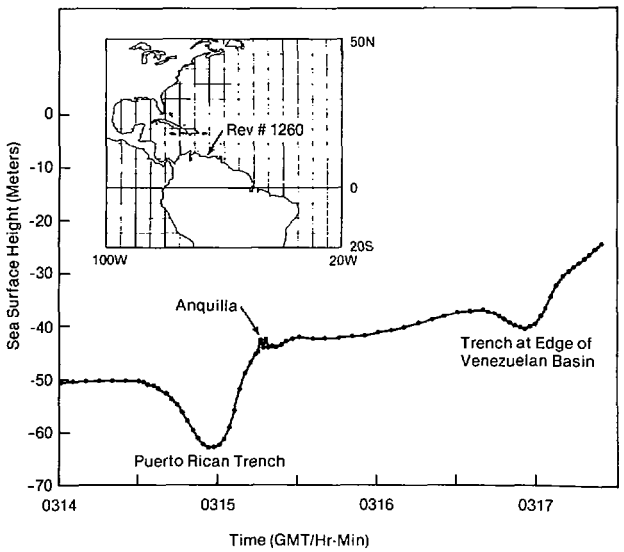

Fig. 12. Sea surface height over trench-type features.

1) Fig. 12 shows a pass during rev #1260 on September 23, 1978, that traversed the Puerto Rican trench area clearly showing the sea surface height depression due to the trench. The disturbance to the immediate right of the trench is due to the island of Anguilla in the Virgin Island chain. Further to the right is a second trench which is located near the southern edge of the Venezuelan Basin. The geoidal rise associated with the continental shelf off the coast of Venezuela can clearly be seen to the right of the second trench.

2) Fig. 13 is taken from a pass that directly overflew Bermuda during rev #1246 on September 22, 1978. The feature in the left part of the sea surface height plot is due to the Gregg sea mount in the New England sea mount chain. This sea mount rises from a surrounding depth of some 5000 m to within approximately 1400 m of the ocean surface. The geoidal rise associated with the island of Bermuda is shown in the right part of the plot.

3) Fig. 14 shows data from rev #1339 on September 28, 1978, that crossed the Gulf Stream south of Cape Hatteras,

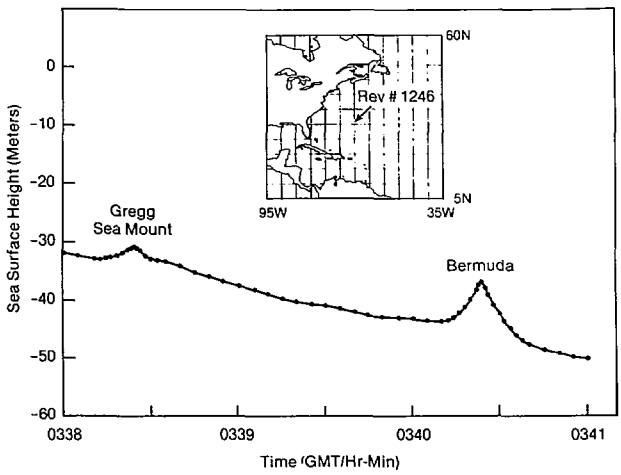

Fig. 13. Sea surface height over sea mount-type features.

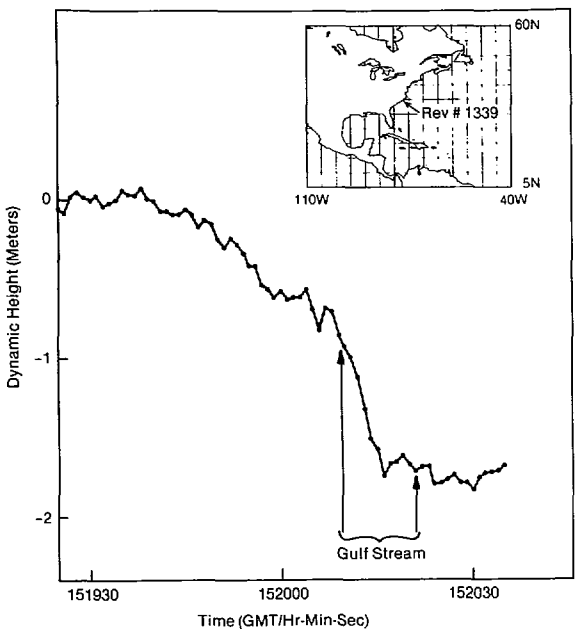

Fig. 14. Dynamic height over Gulf Stream [12].

NC. Plotted is the dynamic height which is the sea surface height with the geoid taken out, thus allowing direct observation of dynamic features such as those due to currents, eddies, storm surges, baratropic effects, etc. The effect of the Gulf Stream as this pass approached the coast of North Carolina is clearly evident. Data has been obtained from the U.S. Naval Oceanographic Office [13] which places the West and East boundaries of the Gulf Stream for the previous day (September 27, 1978) as shown. Agreement, particularly for the Western boundary, is quite good. Note that the slope of the dynamic height is steepest (thus indicating maximum current velocity) near the Western boundary where the Gulf Stream is jammed up against the edge of the Continental Shelf. Also note the almost noise free quality of the data on this exaggerated scale of 0 to −2 m. A 1-s smoothing time was used.

While there are numerous other examples, these should serve to demonstrate the basic height measuring capability

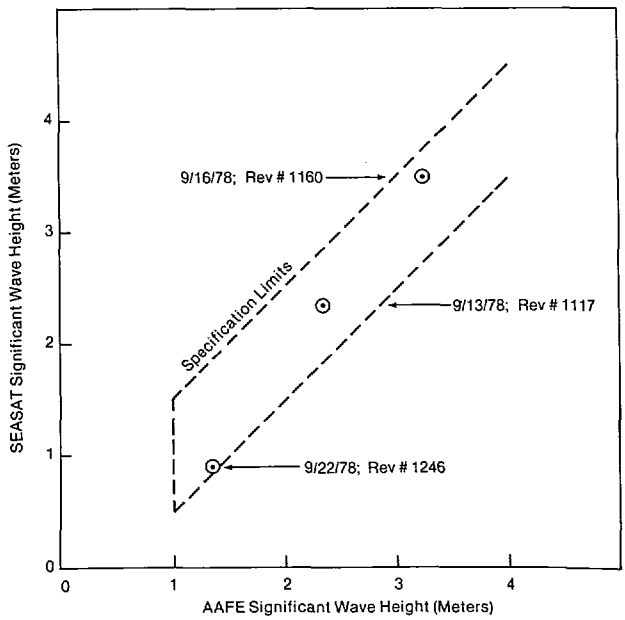

Fig. 15. SWH measurement performance at low SWH (<4 m).

of the Seasat-1 Radar Altimeter system. With its sub 10-cm precision capability, this system has clearly taken a step forward relative to remote sensing of the ocean topography.

C. SWH Measurement Performance

While the absolute calibration of the SWH measurement was not considered to be an engineering assessment task, we did, nonetheless, acquire several sets of surface truth data during the engineering assessment phase. This was done to obtain a quick look at the reasonableness of the SWH measurement prior to the onset of the planned intensive surface truth data collecting activities such as the Gulf of Alaska Seasat Experiment (GOASEX). Surface truth was collected by flying the Wallops C-54 aircraft with the AAFE Altimeter onboard in the footprint of Seasat off the East Coast of the U.S. As noted previously, the AAFE Altimeter development was essentially a breadboard activity leading up to Seasat. Since the Seasat-1 Altimeter is conceptually identical to the AAFE system, the measurements are quite comparable. The AAFE Altimeter was used for this same purpose during the GEOS program and found to provide very accurate measurements of SWH [14].

Fig. 15 shows the results of comparing the Seasat measured SWH with that measured by the AAFE Altimeter during three of the aircraft underflights of Seasat in the vicinity of Bermuda. As can be seen the SWH measurement is within specification for SWH < 4 m which was the highest SWH observed during this quick look exercise. A more extensive SWH calibration validation exercise is currently being conducted by the Seasat-1 Radar Altimeter experiment team (SRAET) and will be reported on at a later data. This activity involves utilizing data obtained during overflights of NOAA buoys, aircraft underflights, and overflights of storms, hurricanes, etc., thus exercising the system in a more exhaustive manner and over a wider range of SWH.

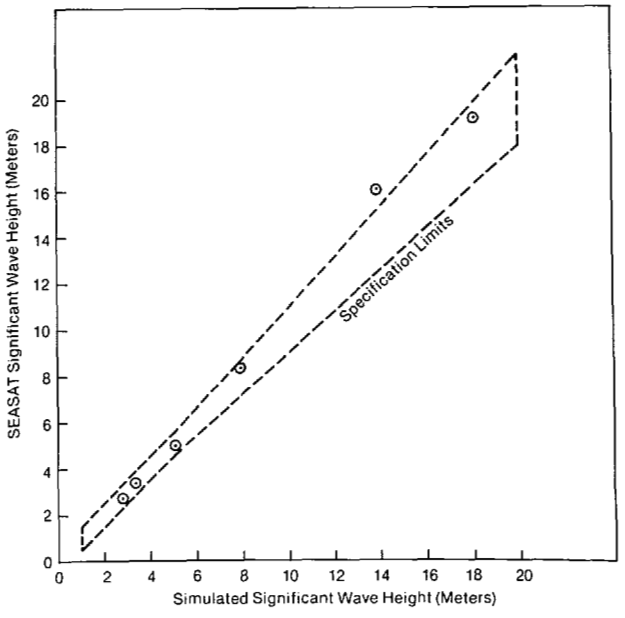

Fig. 16. SWH measurement performance (pre-launch).

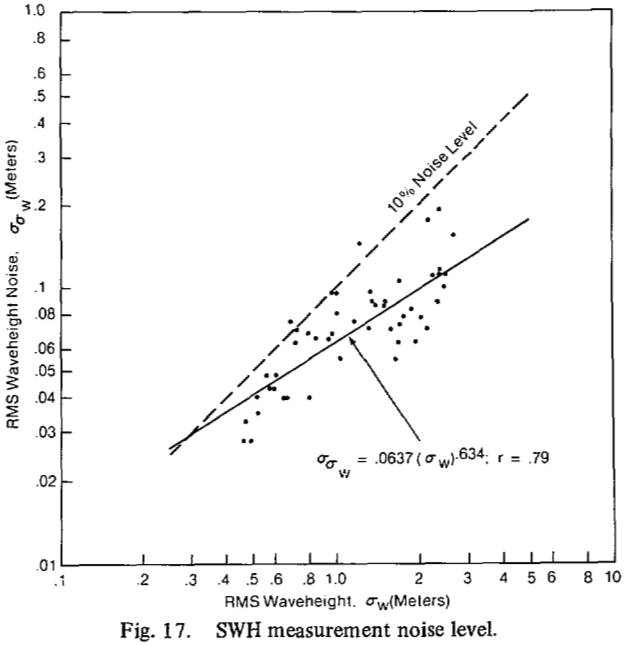

Fig. 17. SWH measurement noise level.

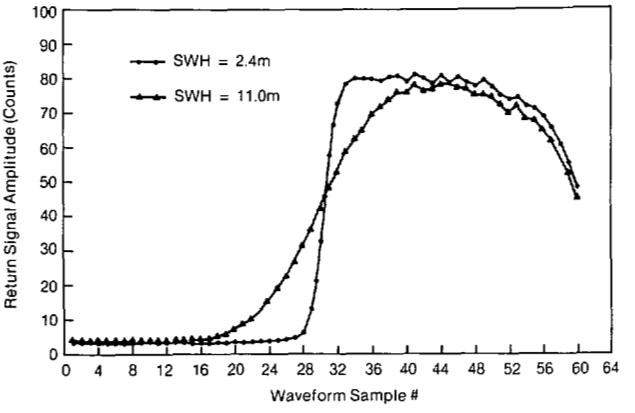

Fig. 18. Return pulse shape as a function of SWH.

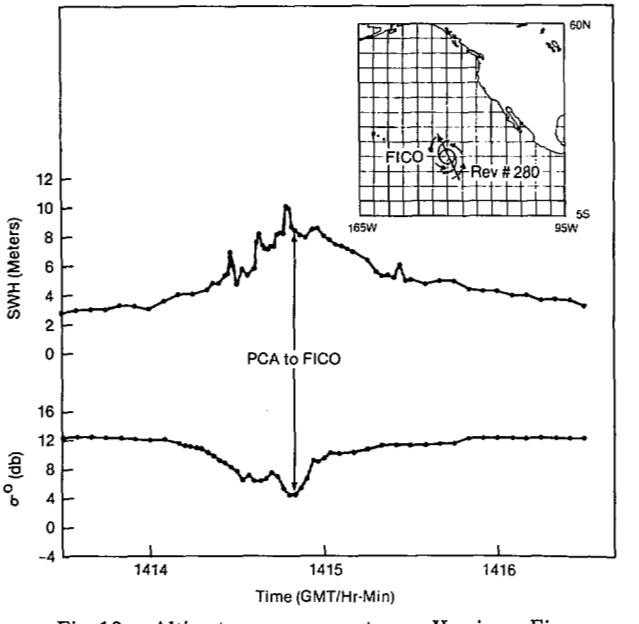

Fig. 19. Altimeter measurements over Hurricane Fico.

To provide some idea of what accuracy might be obtainable at higher SWH, Fig. 16 shows the SWH measurement accuracy based on data obtained during pre-launch testing using the return signal simulator (RSS). Note that the dashed line represents the original performance specification. As can be seen the measured results go slightly (5 percent or so) out of specification around 14-m SWH. Performance otherwise is within specification. Furthermore, even this modest out-of-specification condition can be corrected on the in-flight data by the application of a relatively simple correction factor.

Fig. 17 presents the noise level on the SWH measurement as obtained during the previously noted storm. A power curve has been fit to the data with good results. Note that the noise level increases with sea state as would be expected. Note, also, that the noise level is well below the 10-percent level which was a design goal for the Seasat-1 Altimeter.

Fig. 18 shows typical return waveforms from which SWH measurements are made. The one for a 2.4-m SWH was taken just after passage through the storm previously noted. Note the steep slope of the leading edge. The droop associated with the trailing edge is due primarily to receiver bandpass effects and can be calibrated out if desired. Also shown in Fig. 18 is a return waveform corresponding to an 11-m SWH. It was taken from the peak of the storm. Note that the major difference between this waveform and the previous one for 2.4-m SWH is that the slope of the leading edge has significantly decreased as would be expected. Note also how smooth the data is in both cases based on a 9-s averaging time (two major frames).

Fig. 19 shows SWH measurements obtained during rev #280 on July 16, 1978. This pass came within 100 km of Hurricane Fico between the West Coast of the U.S. and

Hawaii. As can be seen, the peak SWH observed was approximately 10 m.

D. Ocean Backscatter Coefficient (σ°) Measurement Performance

As previously noted, the Seasat-1 Altimeter has an internal calibrate mode which essentially diverts a calibrated portion of the transmit pulse into the receiver for the purpose of AGC and height calibration and stability monitoring. Also, it has been determined that by incorporating internal calibrate mode AGC data into the computation of σ° from in-flight AGC data, the effects of transmit power changes and variation in receiver gain due to temperature are eliminated. The algorithm for accomplishing this is shown below:

$$\sigma^\circ = 39.93 - \mathrm{Cal}_a - \Delta\,\mathrm{AGC}_a + L_{\mathrm{att}} + 30\log_{10}\frac{h}{796.44} + L_{\mathrm{atm}} + B$$

where

σ° = ocean backscatter coefficient dB,
Cal_a = the measured value of the calibrate mode attenuator for step a; there are 11 steps from 0→ 60 dB in 6-dB steps,
$\Delta\mathrm{AGC}_a$ = AGC_a − AGC; i.e., the difference between the calibrate mode AGC for step a and the measured AGC of the ocean surface; a is chosen to minimize $|\Delta\mathrm{AGC}_a|$,
L_{att} = loss in antenna gain at the nadir due to off nadir pointing,
h = the measured altitude km,
L_{atm} = the atmospheric loss dB,
B = bias determined from evaluating on-orbit data dB.

The constant 39.93 dB was determined on the basis of prelaunch thermal-vacuum data (TV#6@APL) taken at seven temperatures (three cold, two ambient, and two hot), five h's, six SWH's, and three σ°'s for a total of 630 different setups overall, over an approximate four day period under vacuum conditions. This constant was determined for each setup and then averaged with a resulting σ of 0.29 dB, thus indicating that it is truly a constant and is stable over all expected operating conditions.

Using the above noted test data set, closure on the algorithm was achieved to within −0.01 dB with a σ of 0.22 dB, thus giving a high degree of confidence in the σ° algorithm.

L_{att} requires knowledge of the antenna pointing angle, currently obtained from spacecraft data to an accuracy of no better than ±0.2°. At an indicated pointing angle of 0.5°, this translates into a potential error in σ° of +1.5 dB to −2.2 dB. Pointing angle data obtained from the altimeter return signal trailing edge slope may be used to improve this.

L_{atm} requires knowledge of local atmospheric conditions along the ground track which could be provided by the Seasat-1 scanning multichannel microwave radiometer (SMMR). Failing this it should probably be set to zero.

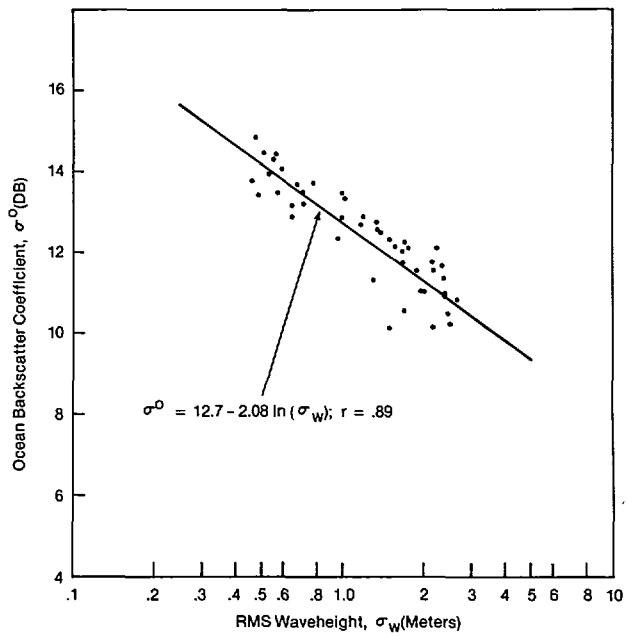

Fig. 20. Ocean backscatter coefficient (σ°) measurement performance.

Based on a preliminary evaluation of data taken during GOASEX and on available GEOS/Seasat intersections a tentative value for B has been established as about −1.5 dB [15]. The source of this bias is not currently understood and is still being evaluated.

Utilizing this algorithm, Fig. 20 shows the relationship obtained between ocean backscatter coefficient (σ°) and SWH. Note that the estimated bias of −1.5 dB has not been applied since it is still under investigation. Again, this data is from the previously noted storm. This time an ln curve has been fit to the data with good results. Note that σ° decreases with SWH as would be expected. The Seasat data has been corrected for measured altitude and pointing angle effects only and not for atmospheric effects.

Referring back to Fig. 19 the σ° as obtained during the Hurricane Fico pass is shown. Note the inverse response to SWH as was seen in Fig. 20. As a point of interest, altimeter measured σ° at nadir has been demonstrated by GEOS to be highly dependent on wind speed and can be routinely used to derive that parameter. In fact, wind speed derived from the GEOS-3 Altimeter measured σ° has been shown to be accurate to ±2 m/s for wind speeds between 4 and 20 m/s [16]. The ability of the Seasat-1 Altimeter to produce this measurement accurately will be subsequently reported on by the SRAET.

E. Measurement Stability

Measurement stability was monitored by the internal calibration mode, which was run approximately once per day for the full mission duration. This mode was used to monitor the stability of the height and AGC measurements, to monitor the transmitter power output, and to monitor the stability of and provide gain correction factors for the waveform sampler data.

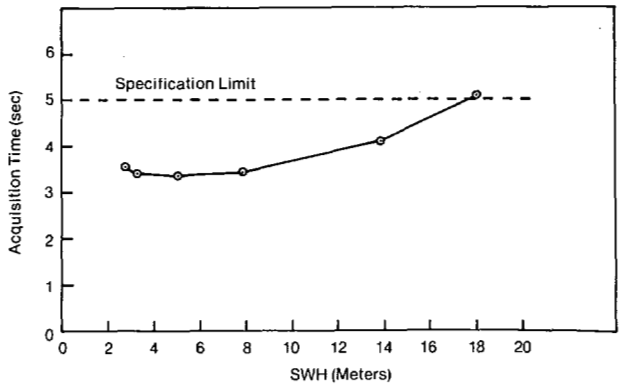

Fig. 21. Acquisition time performance (pre-launch).

An analysis [17] of the data obtained using this mode has shown the measurement stability to be excellent in that, after approximately three months of operation, the indicated shift in the height and AGC measurements was less than 1 cm and 0.1 dB, respectively, and there was essentially no change in the gain of the waveform samplers. Additionally, after 2194 h (including 510 h of pre-launch testing), the transmit power had decreased by approximately 100 W (–0.29 dB) which is in keeping with the 5000-h design life of the tube, i.e., from an output power degradation point of view.

F. Acquisition Time Performance

It was a requirement that the acquisition time, i.e., the time from transmission of the first RF pulse to the time that the basic measurement performance requirements are satisfied, be less than 5 s. This was primarily directed at insuring that quality data was available as quickly as possible after passage from land to water. Fig. 21 shows the acquisition time performance as a function of SWH based on data taken during pre-launch testing. As can be seen, prior to launch, acquisition time was generally around 3.5 to 4 s. A review of the data associated with in-flight acquisition attempts has shown the acquisition time to be generally in agreement with the pre-launch situation. It should be noted that approximately two weeks prior to the death of Seasat, a mode was implemented which essentially added 2.8 s to all acquisition attempts. This came about as a result of using Track Mode 4 to modify the acquisition offset parameter in an attempt to reduce the frequency of occurrence of the occasional transmitter power dropouts over land that had been observed.

G. Hardware Anomalies

During the life of Seasat, there were four hardware anomalies that affected altimeter operation. Two of these were separate instances of altimeter internal temperatures exceeding design limits due to a failure in the spacecraft thermostats controlling internal baseplate heater systems. The primary impact of this was a loss of approximately eight days of data while work around plans were developed, tested, and implemented. A third anomaly occurred when the altimeter transmitter tripped off, as designed, when the spacecraft bus voltage dropped below the design minimum. This was due to a greater than realized drain on the spacecraft power system resulting in dangerously low spacecraft battery voltages during the eclipse period of the orbit. The primary impact of this was a loss of approximately 8.5 days of data while the spacecraft batteries were brought back to a normal and better understood state of charge. The fourth anomaly—and the only true altimeter hardware anomaly—was the problem of occasional transmitter power dropouts over land for periods of approximately 5 s/occurrence after which altimeter operation returned to normal. This was due to improperly implemented acquisition logic that did not allow for the situation where the percentage of valid returns from the surface was extremely low (<8 percent), as sometimes occurred over land. The primary impact of this was the loss of approximately seven days of data while work around plans were developed, tested, and implemented.

H. Data Anomalies

A number of so-called data anomalies have been observed on-orbit. Many of these have been shown to be due to islands, peninsulas, the edge of land boundaries, etc., falling within the altimeter footprint. In this case, the effect shows up first as a change in return pulse shape, due to the higher elevation land in the footprint, which results generally in an increase in AGC, followed by an apparent increase in SWH, and a change (up or down) in height. If the island remains in the footprint for more than a few seconds, this usually results in a loss of lock unless the terrain is relatively smooth and level. This glitch in the data is not a true anomaly in that the altimeter was not designed to handle this condition. Rather the altimeter is intended to acquire data over open ocean where conditions change more gradually. The altimeter response is due to a bona fide surface feature.

Another type of anomaly has been demonstrated, in at least one case [15], to be due to passage over an intense raincell in open ocean. In this case, the effect is evidenced by a decrease in AGC due to signal attenuation through the raincell, followed by a change in height, and an increase in SWH. Typically these raincell crossings last <5 s and no loss of lock occurs. Again, this represents altimeter response to a surface feature.

A third type of anomaly occurring occasionally in open ocean is thought to be due to extremely smooth water resulting in near specular scattering. This type of anomaly shows up as a change in return pulse shape to a narrow high amplitude pulse resulting in an extremely strong increase in AGC, followed by an increase in SWH, and a change in height. Whether or not this effect is really due to extremely smooth water has not currently been verified, but the response is analogous to that observed over the sea ice around Antarctica and Greenland, which is known to be due to near specular scattering.

A fourth type of anomaly has been demonstrated, in at least one case [18], to be due to a spacecraft attitude control system anomaly. The Seasat-1 spacecraft was plagued with attitude control system problems throughout its life and although various work-around plans were implemented, they

were not 100 percent successful in that occasionally the spacecraft attitude would roll or pitch out due to glint in the field of view of the attitude sensing device. This was the case on August 8, 1978, when at approximately 0854 GMT the spacecraft attitude changed by more than 1° ultimately resulting in a loss of altimeter lock for several minutes until the spacecraft attitude came back under control. This showed up in the data as a gradual decrease in AGC with an increase in the trailing edge slope of the return pulse, both due to off nadir pointing, followed by an apparent increase in SWH to its maximum allowable value, and a change in height, all followed shortly thereafter by a loss of lock when the return signal strength became too low to track. This condition persisted for several minutes prior to a resumption of normal operation as the spacecraft attitude reapproached the nadir.

As pointed out, the first three types of anomalies discussed are felt to be due to surface features, and the fourth is due to a spacecraft problem. Fortunately, these types of anomalies occurred infrequently and they were always brief enough such that the data set was not really compromised. In most cases standard editing techniques can be utilized to remove their effect with no regard for their cause. In those cases where this is not practical or desirable, auxiliary data can possibly be used to evaluate their cause and effect.

IV. CONCLUSIONS

Based on the data presented herein it should now be apparent that this system provided high-quality data that contributed to the overall Seasat objectives of demonstrating global monitoring of wave height; detecting currents, tides, and storm surges; and mapping the global ocean geoid. It should also be apparent that the altimeter performed reliably and as designed throughout the three month life of Seasat.

The long-term objective of the 1969 Williamstown Study [2] calling for the development of a 10-cm satellite altimeter system has been met, and the altimeter as a concept has truly come into its own as a reliable oceanographic tool capable of rapidly and remotely sensing the dynamic structure of the ocean surface.

ACKNOWLEDGMENT

The author would like to express his thanks and gratitude to many people who were instrumental in the development and evaluation of the Seasat-1 Radar Altimeter. To the personnel of Hughes Aircraft Company for laying the groundwork for Seasat by developing, under Wallops direction, a 10-cm aircraft altimeter system and to the AAFE program for supporting that effort. To the personnel of the APL and especially to J. MacArthur whose dedication and innovativeness allowed the realization of a 10-cm satellite altimeter system. To C. Purdy and D. Hancock of Wallops who, with the author, put in more hours than any of us care to remember so that the best possible set of altimeter data could be obtained. And to R. Forsythe of Wallops who was largely responsible for the creation of an independent altimeter data processing capability at Wallops such that a timely assessment of on-orbit performance could be obtained.

REFERENCES

[1] "SEASAT-1 Radar Altimeter Phase I engineering assessment report," NASA Wallops Flight Center, Dec. 1978.
[2] "The terrestrial environment: Solid earth and ocean physics," Williamstown Rep. M.I.T., Cambridge, MA, NASA CR-1579, Apr. 1970.
[3] "Updated technical plan for the SEASAT-A Radar Altimeter," APL/JHU, SDO-4099, Rev. A, July 1975.
[4] "Performance specification for the SEASAT-A Radar Altimeter," APL/JHU, 7242-9000, Issue A, Sept. 1977.
[5] J. L. MacArthur, "Design of the SEASAT-A Radar Altimeter," in *Proc. Oceans 76*, Sept. 1976.
[6] J. L. MacArthur, "SEASAT-A Radar Altimeter design description," APL/JHU, SDO-5232, Nov. 1978.
[7] S. W. McCandless and V. J. Cardone, "SEASAT-A oceanographic data system and users," presented at I.A.F. 27th Congress (Anaheim, CA, Oct. 1976).
[8] P. C. Marth, "Generation of the sea state look-up table for the radar altimeter adaptive tracker unit," APL/JHU Internal Memorandum S3R-76-256, Dec. 14, 1976.
[9] L. S. Miller and G. S. Brown, "Engineering studies related to the GEOS-C Radar Altimeter," NASA CR-126462, May 1974.
[10] R. L. Brooks, N. A. Roy, and H. R. Stanley, "Sea ice boundary determination from satellite radar altimetry," presented at the 1978 Spring AGU Conf.
[11] W. J. Pierson, Jr., and E. Mehr, "Average return pulse form and bias for the S193 Radar Altimeter on SKYLAB as a function of wave conditions," *Geophys. Monogr. Ser., Amer. Geophys. Union*, vol. 15, pp. 217–226, 1972.
[12] C. D. Leitao and C. G. Parra, private communication, Aug. 1979.
[13] "Experimental ocean frontal analysis for September 27, 1978," U.S. Naval Oceanographic Office.
[14] C. L. Parsons, "GEOS-3 wave height measurements: An assessment during high sea state conditions in the North Atlantic," *J. Geophys. Res.* vol. 84, no. B8, pp. 4011–4020, July 1979.
[15] "SEASAT Gulf of Alaska workshop report," vol. 1, Panel Rep., JPL 622-101, Apr. 1979.
[16] G. S. Brown, "Correlation of $\sigma 0(0°)$ inferred from wind speed estimates with NOAA hindcast data," NASA CR-141437, Mar. 1978.
[17] W. F. Townsend, "An initial assessment of the performance achieved by the SEASAT-1 Radar Altimeter," to be published as NASA TM-73279.
[18] A. J. Treder, private communication, July 1979.